



Low-light image enhancement using gamma correction prior in mixed color spaces



Jong Ju Jeon^a, Jun Young Park^b, Il Kyu Eom^{b,*}

^a Digital Analysis Division, National Forensic Service, 10, Ipcchun-ro, Wonju-si, Gangwon-do, 26460, Republic of Korea

^b Department of Electronics Engineering, Pusan National University, 2, Busandaehak-ro 63beon-gil, Geumjeong-gu, Busan, 46241, Republic of Korea

ARTICLE INFO

Keywords:

Low-light image enhancement
Gamma correction prior
Mixed color spaces
Transmission map
Inverted image
Atmospheric scattering model

ABSTRACT

In this paper, we propose an efficient and fast low-light image enhancement method using an atmospheric scattering model based on an inverted low-light image. The transmission map is derived as a function of two saturations of the original image in the two color spaces. Due to the difficulty in estimating the saturation of the original image, the transmission map is converted into a function of the average and maximum values of the original image. These two values are estimated from a given low-light image using the gamma correction prior. In addition, a pixel-adaptive gamma value determination algorithm is proposed to prevent under- or over-enhancement. The proposed algorithm is fast because it does not require the training or refinement process. The simulation results show that the proposed low-light enhancement scheme outperforms state-of-the-art approaches regarding both computational simplicity and enhancement efficiency. The code is available on <https://github.com/TripleJ2543>.

1. Introduction

Images captured under low-light conditions have poor visibility characteristics due to insufficient incident radiance. Furthermore, low-light images exhibit reduced contrast, faint colors, narrow pixel ranges, and blurred scenes. Fig. 1(a) shows the sample low-light images and their histograms. The pixel values of the images are shown to be concentrated in the lower range. Since the color difference between the corresponding pixels is small, distinguishing the details in the low-light image is difficult, and the color is faint. Computer vision applications, such as classification, recognition, and understanding of patterns based on images, are often difficult to ensure reliability in adversarial low-light environments.

Low-light image enhancement (LIE) aims to improve the image contrast and detail and recover the image brightness while preventing noise amplification and achieving real-time performance. It is applied in various areas, including autonomous vehicles [1], human pose recognition [2], and facial recognition [3], in low-light environments. Numerous enhancement studies [4] have been conducted, and in particular, machine learning-based LIE methods [5] have been actively studied recently. LIE methods can be roughly divided into classical techniques [6,7], Retinex theory [8], atmospheric scattering model

(ASM) [9], and machine learning. These enhancement algorithms are briefly reviewed in the next section.

In this paper, we focus on ASM-based LIE. ASM is a physical image degradation model widely used in computer vision and image processing, particularly in the image dehazing framework. ASM can be applied to LIE by inverting low-light images. This framework requires accurate transmission map estimation. The primary objective of this study is to propose an efficient method for estimating the transmission map that is fast, pixel-adaptive, and can be computed in a closed-form manner. In our previous work [9], the transmission was derived in the closed form of a single unknown saturation component in the hue, saturation, and value (HSV) color spaces. For a selected saturation stretch function, an adaptive shape of the saturation stretch function for an image was proposed. Our previous method produced acceptable and competitive enhancement results. However, it had limitations in that the proper stretch function should be selected and many parameters should be decided. In this paper, we aim to address the limitations of our method. Hence, we present a novel and faster ASM-based LIE method with only a single tunable parameter and without selection of saturation stretch function using the gamma correction prior (GCP) [10]. The main contributions of our study are as follows:

* Corresponding author.

E-mail address: ikeom@pusan.ac.kr (I.K. Eom).

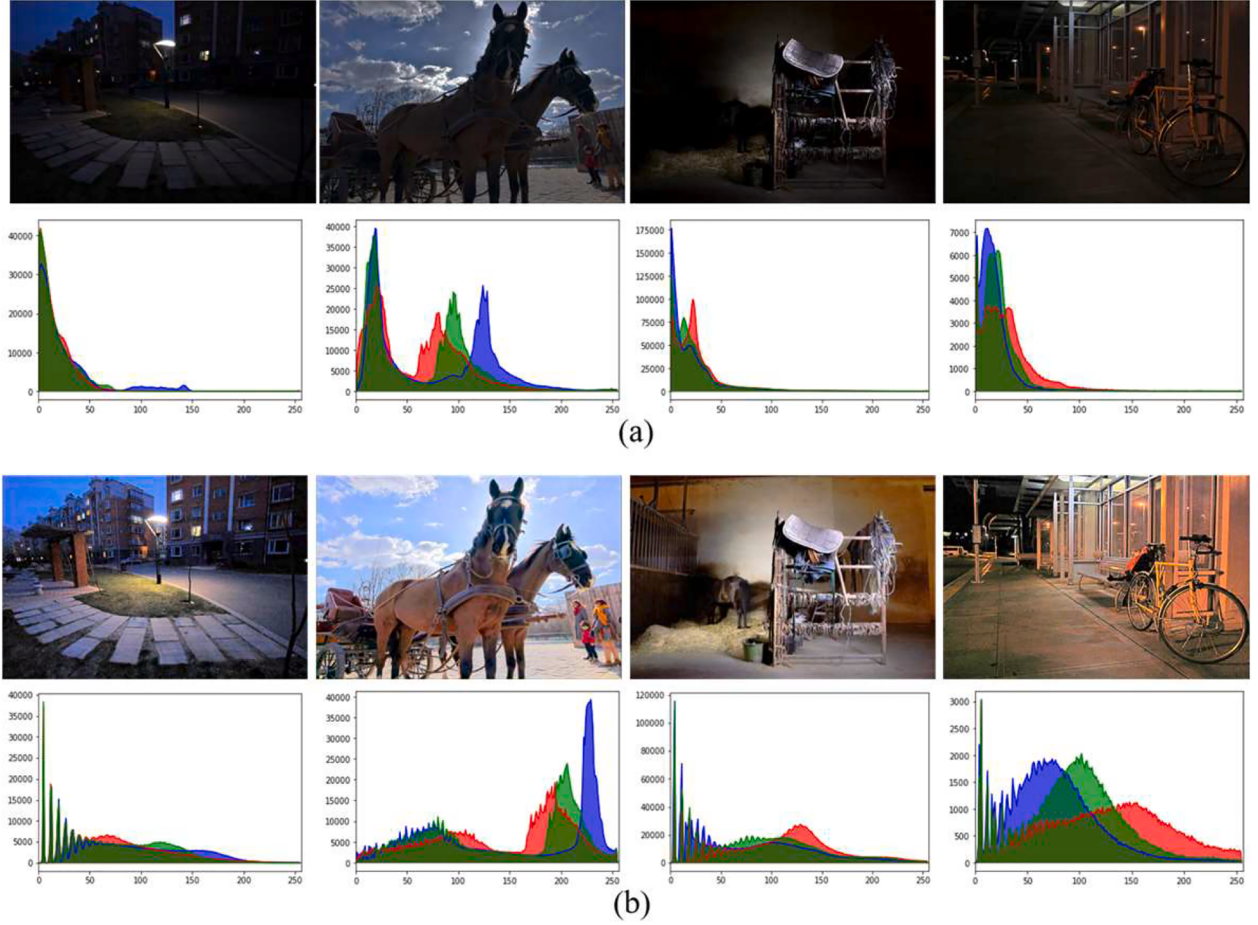


Fig. 1. Low-light images and their enhanced version with histograms. (a) low-light image, and (b) enhanced image using the proposed method.

- The transmission map in the ASM is estimated in two color spaces: hue, saturation and intensity (HSI) and HSV. The estimated transmission is derived in a closed form, comprising two unknown saturation components of the original image in the HSI and HSV color spaces.
- The estimated transmission map comprising two unknown saturation components is reconstructed as a function of the maximum and intensity values of the original image. These two values are estimated through the GCP used in image dehazing. Since the GCP uses the inverse strategy and the inverted low-light image looks resembles the hazy image, it can be applied directly to the proposed method.
- Fixed gamma values can induce over- or under-enhancement because low-light images have various lighting environments. Therefore, we introduce a locally adaptive gamma value generation algorithm because a small gamma value is used for pixels with high illuminance, while a large gamma value is used for pixels with low illuminance.

The presented approach introduces a novel method for estimating the transmission map by utilizing saturation components in two color spaces along with GCP. The proposed method is fast, does not involve training or refinement stages, while achieving satisfactory results for a wide range of low-light images. Fig. 1(b) illustrates the enhanced images obtained using the proposed method and their histograms. The histograms are spread widely, and the color differences of the corresponding pixels increase. Consequently, the brightness and details are restored. In addition, the color sharpens, and the contrast is improved. These results show that the proposed algorithm can be a solution to LIE.

The remainder of this paper is organized as follows. Section 2

provides a brief review of the LIE methods. The derivation of the transmission map based on the saturations in the two color spaces and the transmission map estimation using the GCP are presented in Section 3. The results and discussions of the experiments are presented in Section 4. Finally, concluding remarks are presented in Section 5.

2. Related works

2.1. Classical method

The pixel transform-based method is a spatial domain image enhancement algorithm that converts pixel values into other values through a mathematical function. Nonlinear functions, such as hyperbolic tangent [11], and sigmoid transfer functions [12], have been introduced to enhance image contrast. Pixel transform-based methods have the advantages of simple implementation and high speed. However, these algorithms do not consider the overall image distribution resulting in poor adaptability and limited enhancement performance.

The histogram-based approach [13] is a classic image enhancement method that can preserve or alter background intensity and modify an image histogram to enhance image quality. However, this approach frequently results in excessive contrast enhancement. A contextual and variational contrast enhancement method (CVC) [14] is proposed using a two-dimensional histogram of the input image. In this method, a smooth target histogram is obtained by minimizing the sum of Frobenius norms of the differences between the input and uniformly distributed histograms. However, this algorithm does not fully recover image brightness.

Fu et al. [15] proposed an image enhancement algorithm based on

fusing the results of multiple enhancement techniques (MF). MF integrates multiple image enhancement techniques based on the sigmoid function and adaptive histogram equalization using a linear weighted fusion strategy. However, it is too complex to satisfy real-time requirements. Ying *et al.* [16] presented a bio-inspired dual-exposure fusion algorithm to provide accurate contrast and lightness enhancement (BIMEF). In this method, the source image was generated based on a simulated camera response model, and the weight matrix for image fusion was designed using illumination estimation techniques. However, BIMEF did not fully recover the brightness of the image and exhibited a dimmed color.

The direct image enhancement method [17] establishes a contrast measurement and enhances the image by improving this measurement. It can provide improved image contrast and visually pleasing high-frequency components, however, it can suffer from noise amplification and under- or over-enhancement problems. Combined enhancement approaches have been reported, which offer the advantages of histogram-based and direct methods in discrete cosine [18] and discrete wavelet [19] transform domains. In these algorithms, the high-frequency coefficients are scaled, and the low-frequency coefficients are modified to enhance image contrast. However, these methods occasionally fail, producing color breakage and under- or over-enhancement.

2.2. Retinex method

The Retinex theory [20] provides a flexible framework for LIE tasks. Initially, the single-scale Retinex method [21] was proposed to enhance low-light images. However, this approach produces a halo effect at the edges of the image and causes a colored image to appear grayish due to the contrast enhancement performed in each color channel. To solve this problem, various multiscale Retinex methods [22] and variational Retinex models [23] have been proposed. However, these algorithms can neither prevent color distortion in the resulting image nor reduce noise amplification or the halo effect near the image edge.

Several Retinex-based LIE approaches have been applied to simultaneously estimate illumination and reflectance. Fu *et al.* [24] proposed a probabilistic method for LIE that simultaneously estimates the illumination and reflectance (SRIE) in the linear domain through a maximum *a posteriori* formulation, using prior information on the illumination and reflectance. This method is suitable for properly illuminated objects in low-light images, however, its success is limited when applied to darker regions of an image. Li *et al.* [25] presented a robust Retinex model to improve the enhancement of low-light images containing intensive noise. Their study focused on the inherent noise present in dark regions and offered a reasonable enhancement with good color consistency. However, their results showed image degradation due to over-smoothing. Hao *et al.* [26] proposed an LIE method based on semi-decoupled Retinex image decomposition (SDD). In this method, illumination is gradually estimated using only the input image by applying a Gaussian total variation model. The reflectance was jointly estimated using the input image and intermediate illumination. SDD achieved good qualitative and quantitative performance on public datasets. However, it showed limited performance in generating enhanced images at the semantic and aesthetic-aware levels.

Retinex-based enhancement methods that simultaneously estimate illumination and reflectance may not be suitable for real-time applications because of their high computational cost. To address this shortcoming, other Retinex-based algorithms have been proposed to estimate illumination, which is then used to estimate reflectance. The restored image is obtained from the product of illumination and reflectance. Wang *et al.* [27] proposed a bright-pass filter that was applied with neighborhood brightness information to maintain the naturalness of an image (NPE). This method improves the image contrast and maintains the natural brightness without requiring naturalness preserved enhancement. The NPE maintains naturalness at the cost of illumination

improvement, hence, it may not adequately enhance darker regions. Guo *et al.* [28] proposed an image enhancement algorithm that uses illumination map estimation (LIME) to estimate the initial illumination by considering the pixel-wise maximum of all the color channels of the low-light image. Subsequently, it computed the refined illumination by optimizing a multiobjective problem. Although LIME exhibits a strong performance, over-enhancement occurs in the properly illuminated regions of low-light images. Ren *et al.* [29] introduced an enhancement method combining the camera response model and the traditional Retinex model (LECARM). Through LECARM, enhanced images were obtained by locally adjusting the exposure of the low-light images. This method achieved acceptable performance despite a slightly lower brightness recovery.

2.2. ASM method

Based on the ASM [30], LIE attempts to estimate the transmission map by exploiting the similarity between inverted low-light images and haze images. Shi *et al.* [31] applied the dark channel prior (DCP)-based dehazing method [32] to an inverted low-light image, achieving acceptable visual quality. Gu *et al.* [33] proposed a new low-light image degradation model derived from ASM. They presented a physically valid image prior, a statistical regularity of extensive, natural clear images. However, these two ASM-based approaches have the disadvantage of over-enhancement, which brightens all areas of the image. Recently, we presented an LIE algorithm using an inverted image normalized by atmospheric light (IINAL) [9]. In this method, the medium transmission was only derived as a function of the saturation of the scene radiance, and the image-adaptive saturation of the scene radiance was estimated through a simple stretch function following the average saturation of the low-light image. Although IINAL produced an acceptable performance, it required several parameters that affected enhancement performance and had the problem of selecting a proper saturation stretch function.

ASM-based LIE schemes can provide acceptable enhancement performance with low computational complexity. However, these approaches require some prior information because ASM causes an ill-posed problem. The inverted low-light images have unique characteristics. Thus, there is still opportunity to develop a suitable LIE method rather than directly applying the haze removal method.

2.4. Machine learning method

Recently, LIE techniques using machine learning have attracted significant attention. Lore *et al.* [34] presented a stacked autoencoder that performs patch-based LIE and denoising (LLNet). Although LLNet achieved reasonable brightness recovery, it generated dimmed colors and did not recover image details. Wei *et al.* [35] proposed a deep RetinextNet that includes decomposition and enhancement networks for illumination adjustment. However, this method can cause a significant color shift and unrealistic artifacts. Guo *et al.* [36] designed a zero-reference deep curve estimation (Zero-DCE) that determines light enhancement through image-specific curve estimation using a deep network. Zero-DCE exhibited slightly lower brightness recovery and weak detail information. Lv *et al.* [37] introduced an end-to-end attention-guided method based on a multibranch convolutional neural network (AGLLNet). However, AGLLNet generated annoying artifacts and faded colors in the enhanced images. Jiang *et al.* [38] proposed an unsupervised generative adversarial network (EnlightenGAN). EnlightenGAN was trained without low- and normal-light image pairs. It used normalizing paired training using the information extracted from the input itself and benchmarking a series of innovations in LIE problems. EnlightenGAN produced reasonable brightness and detail recovery and can be easily adapted to enhance real-world images in various domains. Recently, Wang *et al.* [39] proposed a conditional normalizing flow (LLFlow) to model the conditional distribution of normally exposed images and introduced a module to extract the illumination-invariant

color map inspired by Retinex theory. LLFlow achieved acceptable quantitative and qualitative results for the existing benchmark datasets.

Popular supervised learning structures require large-scale training datasets comprising low-light images of inputs and normal images as ground truths. However, the performance of machine learning-based methods is often degraded due to untrained image data. Hence, machine learning-based LIE is still a challenging task because there is an opportunity for improvement [5].

3. Proposed method

3.1. ASM for LIE

In the dehazing framework, the observed hazy image is modeled as a convex sum of the scene radiance and atmospheric light. This formation is described using ASM [30]. Let $\mathbf{O}(x)$ be the observed low-light image, where x is the position of the pixel within the image. In order to obtain the inverted image and estimate the transmission map, the low-pass filtered image \mathbf{I} is used instead of \mathbf{O} to eliminate small noise. To effectively mitigate small noise present in \mathbf{O} , a 7×7 Gaussian kernel is employed. Given that the inverted low-light image $\mathbf{1} \cdot \mathbf{I}(x)$ resemble a hazy image, the ASM for the inverted low-light image is expressed as follows:

$$\mathbf{1} - \mathbf{I}(x) = (\mathbf{1} - \mathbf{J}(x))t(x) + \mathbf{A}(1 - t(x)), \quad (1)$$

where $\mathbf{J}(x)$ is the original image to be restored, \mathbf{A} is the atmospheric light estimated from $\mathbf{1} \cdot \mathbf{I}(x)$, and $t(x)$ is the transmission map, assumed to be the same for the three color channels. In this paper, boldface symbols are used to represent vectors with three color components. The goal of the ASM for LIE is to recover $\mathbf{J}(x)$ from $\mathbf{O}(x)$. Hence, $\mathbf{J}(x)$ can be recovered from a single image if the transmission map and atmospheric light are estimated as follows:

$$\mathbf{J}(x) = \frac{\mathbf{O}(x) - \mathbf{1} + \mathbf{A}}{t(x)} + \mathbf{1} - \mathbf{A}. \quad (2)$$

Since \mathbf{A} can be easily estimated, the accurate estimation of $t(x)$ is essential in ASM-based LIE.

3.2. Transmission map estimation

In this study, we aim to estimate a pixel-level transmission map. The ASM equation shown in (1) is normalized by \mathbf{A} as follows:

$$\frac{\mathbf{1} - \mathbf{I}(x)}{\mathbf{A}} = \frac{\mathbf{1} - \mathbf{J}(x)}{\mathbf{A}}t(x) + 1 - t(x). \quad (3)$$

To simplify the expression, we let $\mathbf{L}(x) = (\mathbf{1} - \mathbf{I}(x)) / \mathbf{A}$ and $\mathbf{R}(x) = (\mathbf{1} - \mathbf{J}(x)) / \mathbf{A}$. $\mathbf{L}(x)$ and $\mathbf{R}(x)$ are the inverted low-light image and inverted scene radiance normalized by \mathbf{A} , respectively. The relationship in (3) has the following form:

$$\mathbf{L}(x) = \mathbf{R}(x)t(x) + 1 - t(x) \quad (4)$$

Since the estimated $t(x)$ from (4) is an ill-posed problem, prior information, such as the DCP [32], can be applied to obtain $t(x)$ values. The DCP assumes that the darkest intensity within a predefined patch is 0. This assumption can induce to unsuccessful enhancements that require additional post-processing or refinement processes.

In this study, we use the pixel-level maximum operation in (4), assuming that $t(x)$ is identical for all color channels. According to the maximum operation, the following relationship is obtained:

$$\max_c \mathbf{L}(x) = \max_c \mathbf{R}(x)t(x) + 1 - t(x), \quad (5)$$

where $c = \{\text{red, green, blue}\}$. For example, the $\max_c \mathbf{L}(x)$ operation returns a single maximum value of the red, green, and blue values of $\mathbf{L}(x)$. From (5), we can obtain the transmission map as follows:

$$t(x) = \frac{1 - M_L(x)}{1 - M_R(x)}, \quad (6)$$

where $M_L(x) = \max_c \mathbf{L}(x)$ and $M_R(x) = \max_c \mathbf{R}(x)$. To obtain $t(x)$, $M_R(x)$ should be determined. However, the direct estimation of $M_R(x)$ is a difficult task. We use two saturation values in the HSI and HSV color spaces to estimate the transmission map. Saturation-based transmission map estimation algorithms with the minimum operation in (4) were proposed in the HSV [9] color space and were successfully applied to LIE.

In the HSI color space, the saturation value of $\mathbf{R}(x)$, $S_R^{HSI}(x)$ is defined as follows:

$$S_R^{HSI}(x) = 1 - \frac{m_R(x)}{\mu_R(x)}, \quad (7)$$

where $m_R(x)$ is the minimum value and $\mu_R(x)$ is the average value of the three color values at location x . The saturation value $S_R^{HSV}(x)$ in the HSV color space for $\mathbf{R}(x)$ is defined as follows:

$$S_R^{HSV}(x) = 1 - \frac{m_R(x)}{M_R(x)}. \quad (8)$$

From (7) and (8), the following relationships are derived:

$$m_R(x) = (1 - S_R^{HSI}(x))\mu_R(x), \quad (9)$$

$$m_R(x) = (1 - S_R^{HSV}(x))M_R(x), \quad (10)$$

By equating (9) and (10), we can derive the following equation:

$$M_R(x) = \mu_R(x) \frac{1 - S_R^{HSI}(x)}{1 - S_R^{HSV}(x)}. \quad (11)$$

By applying the processes outlined in (7) to (11) to $\mathbf{L}(x)$, $M_L(x)$ is be obtained as follows:

$$M_L(x) = \mu_L(x) \frac{1 - S_L^{HSI}(x)}{1 - S_L^{HSV}(x)}, \quad (12)$$

where $\mu_L(x)$ is the average value of the color values of $\mathbf{L}(x)$, and $S_L^{HSI}(x)$ and $S_L^{HSV}(x)$ are the saturation values of the HSI and HSV color spaces, respectively. Using (11) and (12), we can obtain the transmission map of (6) as follows:

$$t(x) = \frac{1 - \mu_L(x) \frac{1 - S_L^{HSI}(x)}{1 - S_L^{HSV}(x)}}{1 - \mu_R(x) \frac{1 - S_R^{HSI}(x)}{1 - S_R^{HSV}(x)}}. \quad (13)$$

There are three unknowns: $\mu_R(x)$, $m_R(x)$, and $M_R(x)$ in (13). The unknown value $\mu_R(x)$ is calculated using the average operation in (4) as follows:

$$\mu_L(x) = \mu_R(x)t(x) + 1 - t(x). \quad (14)$$

Therefore, $\mu_R(x)$ is obtained as follows:

$$\mu_R(x) = \frac{\mu_L(x) - 1}{t(x)} + 1. \quad (15)$$

By substituting (15) into (14), $t(x)$ is calculated as follows:

$$t(x) = \frac{1 - \mu_L(x) \frac{1 - S_L^{HSI}(x)}{1 - S_L^{HSV}(x)}}{1 - \left(\frac{\mu_L(x) - 1}{t(x)} + 1 \right) \frac{1 - S_R^{HSI}(x)}{1 - S_R^{HSV}(x)}}. \quad (16)$$

This is a first-order equation for $t(x)$ that is analytically calculated as follows:

$$t(x) = 1 - \mu_L(x) \frac{(1 - S_L^{HSI}(x))(1 - S_R^{HSV}(x)) - (1 - S_L^{HSV}(x))(1 - S_R^{HSI}(x))}{(1 - S_L^{HSV}(x))(1 - S_R^{HSV}(x)) - (1 - S_L^{HSI}(x))(1 - S_R^{HSI}(x))}. \quad (17)$$



Fig. 2. Recovered low-light images using virtual processed images $V(x)$ with various Γ values.

In summary, the estimated $t(x)$ is a function of two saturations in the HSI and HSV color spaces. However, estimating S_R^{HSI} and S_R^{HSI} is a difficult task because direct estimation of the two saturations requires some inequality constraints and determination of saturation stretch functions [9]. In this paper, we propose an efficient estimation of $t(x)$ using GCP.

3.3. Gamma correction prior

In the dehazing framework, GCP [10] was proposed using the inverse strategy. This prior is based on the assumption that the inverted hazy image is also visually similar to the low-light images. The GCP is expressed as follows:

$$\mathbf{1} - \mathbf{H}_v(x) = (\mathbf{1} - \mathbf{H}(x))^{\Gamma}, \quad (18)$$

where $\mathbf{H}(x)$ is the hazy image, $\mathbf{H}_v(x)$ is the virtual result, and Γ is the gamma correction factor. $\mathbf{H}_v(x)$ is used as an efficient initial image to estimate the transmission map, and is successfully applied to recover hazy images.

In this paper, the GCP is used to estimate the transmission map. Moreover, since $\mathbf{L}(x)$ is the inverted low-light image, it is considered $\mathbf{1} - \mathbf{H}(x)$ in the GCP. We modify the GCP as

$$\mathbf{V}(x) = \mathbf{L}(x)^{\Gamma}, \quad (19)$$

where $\mathbf{V}(x)$ is the processed virtual image, which can be considered as $\mathbf{1} - \mathbf{H}_v(x)$. Using $\mathbf{V}(x)$, a potentially enhanced image can be calculated by applying the relationship $\mathbf{R}(x) = (\mathbf{1} - \mathbf{J}(x))/A$ in (3) as follows:

$$\mathbf{J}_v(x) = \mathbf{1} - \mathbf{A}\mathbf{V}(x), \quad (20)$$

where $\mathbf{J}_v(x)$ is the potentially enhanced image obtained using $\mathbf{V}(x)$. In (20), $\mathbf{R}(x)$, which is the recovered inverted image normalized by A , is

considered as $\mathbf{V}(x)$. Fig. 2 shows the low-light image, $\mathbf{J}_v(x)$, and $\mathbf{J}(x)$ according to various Γ values. The processed virtual images exhibit good restoration performance regarding image intensity and poor performance regarding color or detail recovery. In addition, as the Γ value increases, the intensity is recovered well, while the color and detail are lost. Thus, the intensity information of $\mathbf{V}(x)$ can be effectively used for LIE.

The proposed transmission map shown in (17) comprises two saturation values. By utilizing the definitions of saturation in the HSI and HSV color spaces, the proposed $t(x)$ is described as follows:

$$t(x) = 1 - \mu_L(x) \frac{\frac{m_L(x)}{\mu_L(x)} \frac{m_R(x)}{M_R(x)} - \frac{m_L(x)}{M_L(x)} \frac{m_R(x)}{\mu_R(x)}}{\frac{m_L(x)}{M_L(x)} \frac{m_R(x)}{M_R(x)} - \frac{m_L(x)}{M_L(x)} \frac{m_R(x)}{\mu_R(x)}}. \quad (21)$$

The final simplified form of $t(x)$ is as follows:

$$t(x) = 1 - \mu_L(x) \frac{M_L(x)\mu_R(x) - \mu_L(x)M_R(x)}{\mu_L(x)\mu_R(x) - \mu_L(x)M_R(x)}. \quad (22)$$

The reformed $t(x)$ is a function of the intensity values of the HSI and HSV color spaces. If $\mu_R(x)$ (HSI intensity) and $M_R(x)$ (HSV intensity) are known, then $t(x)$ can be determined.

Two unknown values, $\mu_R(x)$ and $M_R(x)$ are estimated using $\mathbf{V}(x)$ as follows:

$$\mu_R(x) \approx \mu_V(x), \quad (23)$$

$$M_R(x) \approx M_V(x), \quad (24)$$

Finally, $t(x)$ is estimated as follows:

$$t(x) \approx 1 - \mu_L(x) \frac{M_L(x)\mu_V(x) - \mu_L(x)M_V(x)}{\mu_L(x)\mu_V(x) - \mu_L(x)M_V(x)}. \quad (25)$$

The restored image using the estimated $t(x)$ is obtained as

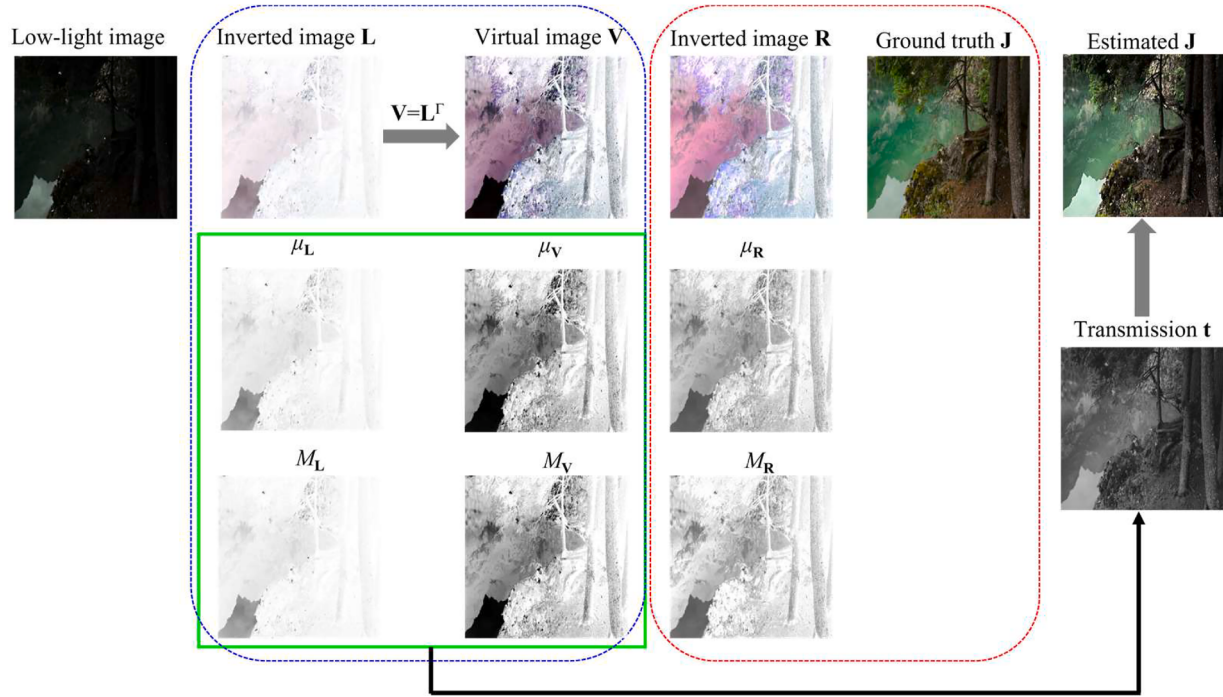


Fig. 3. Sample process for recovering low-light image based on the proposed method.

$$\tilde{J}(x) = \frac{\mathbf{O}(x) - \mathbf{1} + \mathbf{A}}{\max(t(x), t_0)} + \mathbf{1} - \mathbf{A}, \quad (26)$$

where t_0 is a small positive constant to prevent zero division. In general, this is set at 0.1.

Fig. 3 illustrates a sample process for recovering low-light images based on inverted low-light image L and virtual image V . In Fig. 3, the blue dotted box contains image V , from which $\mu_V(x)$ and $M_V(x)$ are calculated. From L , we can calculate V using the GCP and estimate $\mu_V(x)$ and $M_V(x)$. The reference image J and calculated R , $\mu_R(x)$ and $M_R(x)$ are shown in the red dotted box. The estimated pair $\mu_V(x)$ and $M_V(x)$ from V do not look much different from the calculated pair $\mu_R(x)$ and $M_R(x)$ from the inverted reference image R . Using the two known values ($\mu_L(x)$ and $M_L(x)$) and the two estimated values ($\mu_V(x)$ and $M_V(x)$) enclosed by the solid green box, the transmission map is calculated based on (25). The restored low-light image obtained using (26) is depicted at the top-right position.

3.4. Effect of gamma value

As shown in (25), $t(x)$ is a function of $\mu_V(x)$ and $M_V(x)$. Since $\mu_V(x)$ and $M_V(x)$ are determined using the Γ value, the proposed LIE method has a single parameter Γ . Low-light images have various lighting conditions, hence, a single fixed Γ value does not ensure the enhancement of various low-light images. Overall, large Γ values are suitable for images with very low illuminance. Small gamma values can be advantageous for image enhancement with relatively low illuminance.

To determine the relationship between Γ values and low-light images, we performed an experiment using the GLADNet low-light image dataset [40] with ground truth comprising of 5000 image pairs. First, we divided 5000 low-light images into nine groups at 0.1 intervals according to the averaged maximum value (Z_{\max}) of the three color values at the spatial location in the given low-light image. The maximum operation is used to avoid a color pixel with a highly saturated single color being considered a low-light pixel. Second, image enhancement is performed by obtaining $t(x)$ with 21 different Γ values. In this case, the Γ values are used by decomposing from 1 to 11 at 0.5 intervals. Three evaluation measures are tested for the GLADNet dataset, including the

peak signal-to-noise ratio (PSNR), structural similarity index (SSIM) [41], and CIEDE2000 color difference [42]. The SSIM evaluates the ability to preserve the structural information of the algorithms, and the CIEDE2000 evaluates color fidelity. The SSIM ranges from -1 to 1, with a maximum value of 1 for two identical images. Furthermore, CIEDE2000 accurately measures the color difference between two images and generates values ranging from 0 to 100, with smaller values indicating better color preservation.

Fig. 4 shows the three evaluation measures for the GLADNet dataset. The three best-ranked values are highlighted in Fig. 4. As shown in Fig. 4, Γ values with high enhancement performance have an approximately exponential function for the averaged maximum value. In summary, setting the adaptive Γ value according to the given low-light image can induce good enhancement results.

In this paper, we present a simple method for determining the pixel-adaptive gamma value of a low-light image. The pixel-adaptive gamma value $\Gamma(x)$ for each pixel of a low-light image $\mathbf{O}(x)$ is determined as a simple exponentially decreasing function with the maximum (Γ_{\max}) and minimum ($\Gamma_{\min}=1$) limits as follows:

$$\Gamma(x) = ae^{-M_O(x)} + b, \quad (27)$$

where $M_O(x)=\max_c \mathbf{O}(x)$, and a and b are the coefficients that determine the shape of the exponential function, which are

$$a = \frac{\Gamma_{\max} - 1}{1 - e^{-1}}, \quad (28)$$

and

$$b = \Gamma_{\max} - a. \quad (29)$$

Fig. 5 shows the enhancement results obtained using pixel-adaptive $\Gamma(x)$ values. $\Gamma(x)$ is large when the image intensity is low, and small when the image intensity is relatively high. In all simulations, the parameter Γ_{\max} is fixed at six to enhance the low-light images using the proposed method.

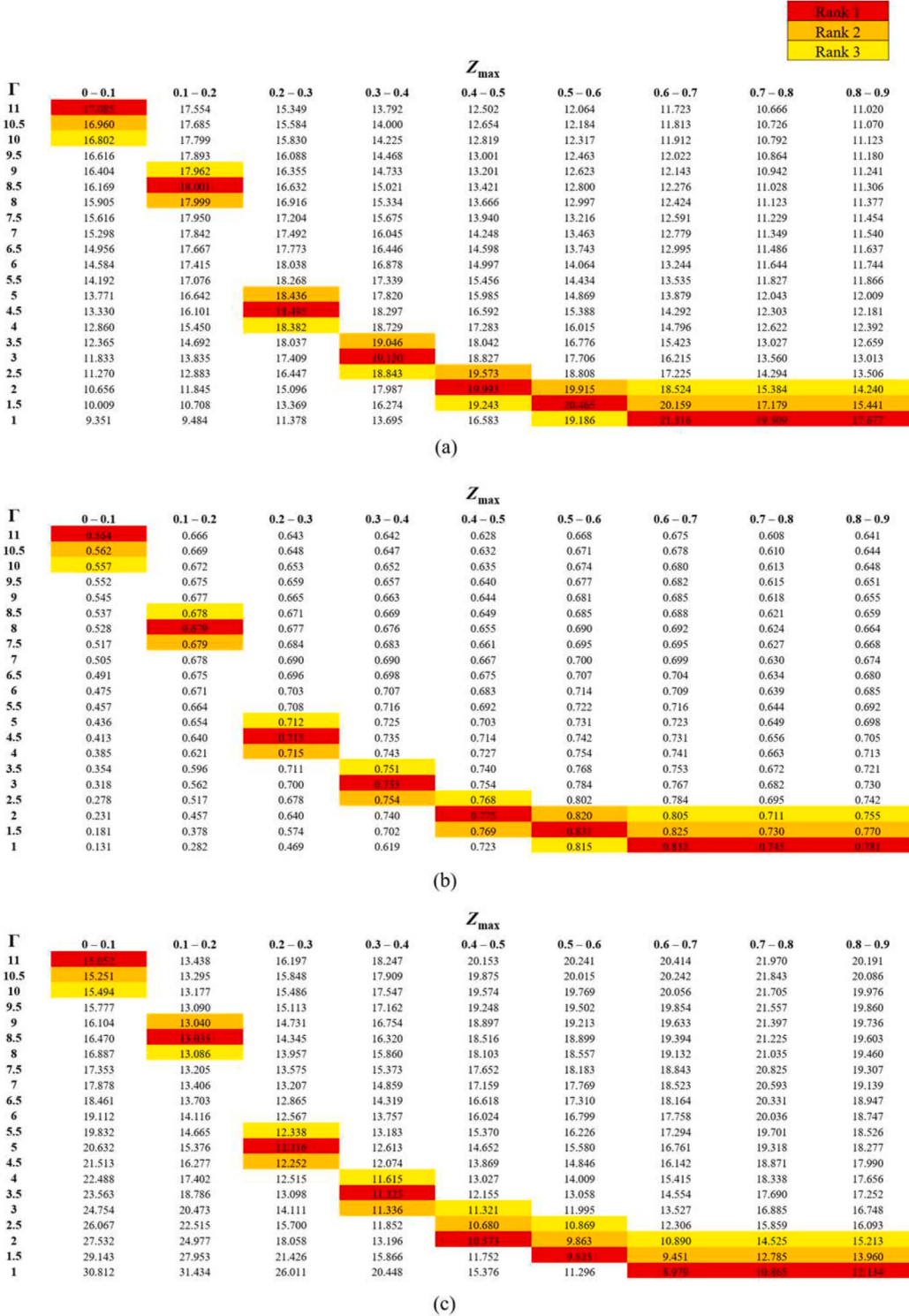


Fig. 4. Highlighted three best-ranked objective measures in low-light image enhancement for GLADNet dataset [40]. (a) PSNR values, (b) SSIM values, and (c) CIEDE2000 values.

4. Simulation results

To evaluate the performance of the proposed enhancement method, 15 state-of-the-art algorithms are selected for comparison based on four categories: classic methods (CVC [14], MF [15], and BIMEF [16]), Retinex methods (SRIE [24], SDD [26], NPE [27], LIME [28], and LECARM [29]), the ASM method (IINAL [9]), and machine learning methods (LLNet [34], RetinexNet [35], Zero-DCE [36], AGLLNet [37],

EnlightenGAN [38], and LLFlow [39]). The codes for the compared enhancement methods were downloaded from their respective project sites.

4.1. Computation time

The proposed method was implemented on an Intel i7-10700K CPU @ 3.80 GHz with 48 GB RAM without multithreading acceleration. Its

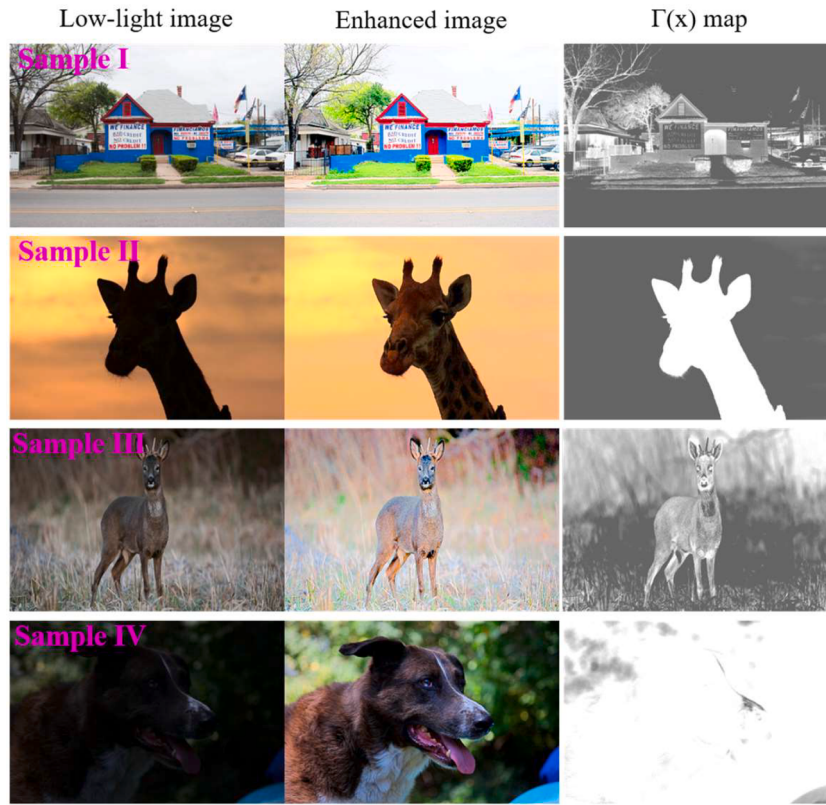


Fig. 5. Low-light image enhancement results for sample images using pixel-adaptive Γ values.

Table 1
Execution times for various algorithms (unit: second).

| Method | Image size | | | | |
|-----------------|--------------|---------------|----------------|----------------|---------|
| | 480 × 640 | 768 × 1024 | 1312 × 2000 | 2048 × 3072 | Average |
| CVC [14] | 0.096 | 0.264 | 0.837 | 2.724 | 0.980 |
| MF [15] | 0.138 | 0.247 | 0.681 | 1.963 | 0.757 |
| BIMEF [16] | 0.067 | 0.159 | 0.507 | 1.356 | 0.522 |
| SRIE [24] | 2.180 | 7.365 | 36.474 | 159.522 | 51.385 |
| SDD [26] | 1.672 | 4.578 | 17.852 | 113.965 | 34.517 |
| NPE [27] | 5.089 | 13.234 | 44.132 | 105.537 | 41.998 |
| LIME [28] | 0.061 | 0.153 | 0.572 | 1.607 | 0.598 |
| LECARM | 0.069 | 0.172 | 0.554 | 1.342 | 0.534 |
| [29] | 0.076 | 0.183 | 0.510 | 1.223 | 0.498 |
| IINAL [9] | | | | | |
| Proposed method | 0.037 | 0.092 | 0.302 | 0.776 | 0.302 |

code was written in nonoptimized Python in the Linux Ubuntu 18.04.6 LTS environment. The comparison methods were implemented in the same environment. The execution time averaged over 20 operations. The durations of image reading and writing were excluded. **Table 1** shows the execution times for various image sizes. The proposed method achieved the fastest execution time for all images. The IINAL scheme had the second-fastest execution time, and its overall average execution time was about 65% slower than that of the proposed algorithm. Retinex-based algorithms, including SRIE, SDD, and NPE have high computational costs.

4.2. Quantitative comparison

For a quantitative comparison, we used the GLADNet dataset [40] with ground truth comprising 5000 image pairs. **Table 2** presents the average performance of various LIE algorithms regarding PSNR, SSIM,

Table 2
Quantitative comparisons of various algorithms using GLADNet dataset [40].

| Quantitative metric | | | |
|---------------------|---------------|--------------|---------------|
| Method | PSNR↑ | SSIM↑ | CIEDE2000↓ |
| CVC [14] | 15.667 | 0.588 | 16.684 |
| MF [15] | 17.777 | 0.741 | 13.049 |
| BIMEF [16] | 17.938 | <u>0.740</u> | 13.347 |
| SRIE [24] | 16.177 | 0.677 | 16.011 |
| SDD [26] | 17.122 | 0.701 | 14.079 |
| NPE [27] | 17.617 | 0.732 | 13.237 |
| LIME [28] | 17.005 | 0.712 | 13.265 |
| LECARM [29] | 17.854 | 0.735 | <u>12.636</u> |
| IINAL [9] | <u>17.941</u> | 0.701 | 12.995 |
| LLNet [34] | 17.005 | 0.653 | 13.535 |
| RetinexNet [35] | 15.435 | 0.668 | 15.675 |
| Zero-DCE [36] | 17.776 | 0.721 | 13.165 |
| AGLLNet [37] | 17.404 | 0.681 | 14.004 |
| EnlightenGAN [38] | 17.504 | 0.697 | 13.679 |
| LLFlow [39] | 17.876 | 0.724 | <u>12.928</u> |
| Proposed method | 18.808 | 0.717 | 12.034 |

and CIEDE2000. The top three performances are highlighted in bold, underlined and italic text. Moreover, the proposed method exhibited the best PSNR and CIEDE2000. The SSIM score of the proposed algorithm ranks seventh out of 16 algorithms. As shown in **Table 2**, classic approaches based on fusion, such as MF and BIMEF achieve high PSNR and SSIM scores. IINAL has a high PSNR score, and LECARM and LLFlow achieve good color restoration. CVC and SRIE have low quantitative scores. In summary, the proposed method, IINAL, LECARM, MF, BIMEF, and LLFlow, achieve good scores for full-reference image quality measures.

Fig. 6 presents the comparison of the enhanced image quality with our proposed method and those of state-of-the-art LIE methods. This shows that CVC fails to restore brightness and recover color information. Moreover, MF, BIMEF, SRIE and SDD do not fully recover the brightness

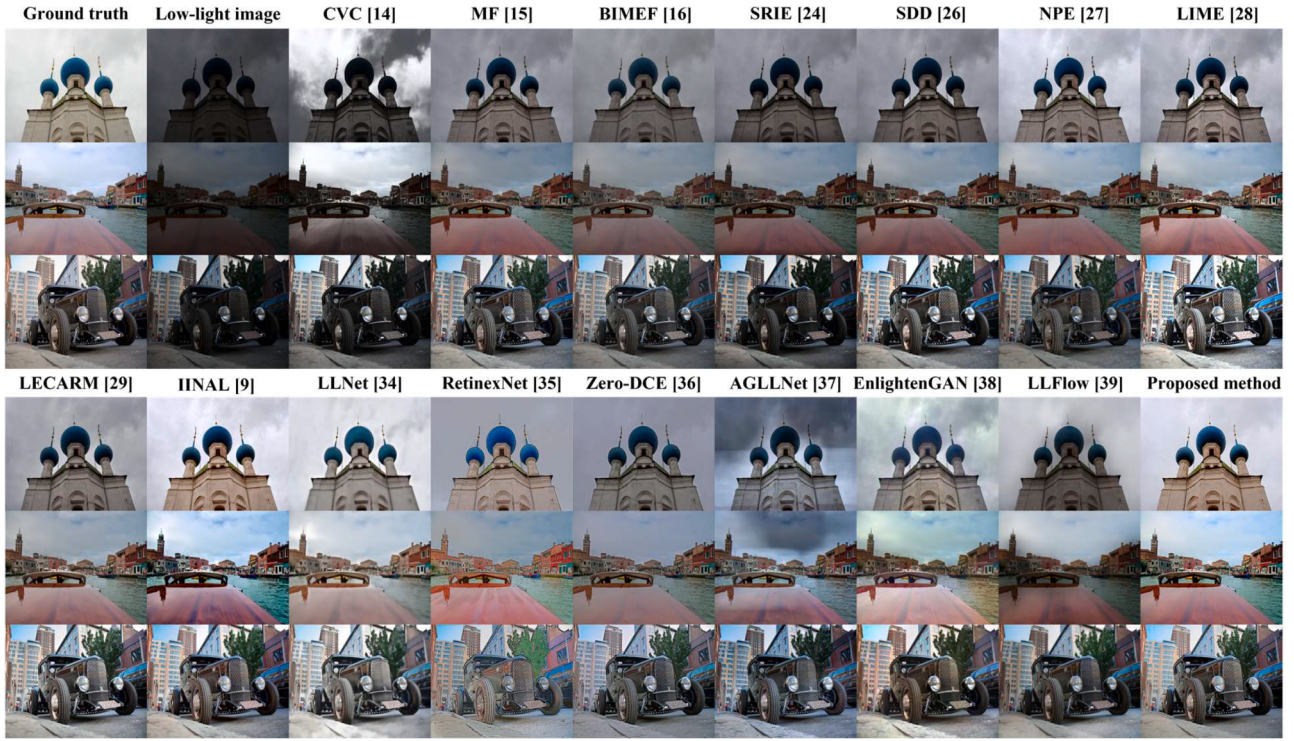


Fig. 6. Sample low-light image restoration results for GLADNet dataset [40], which has 5000 low-light and ground truth image pairs.

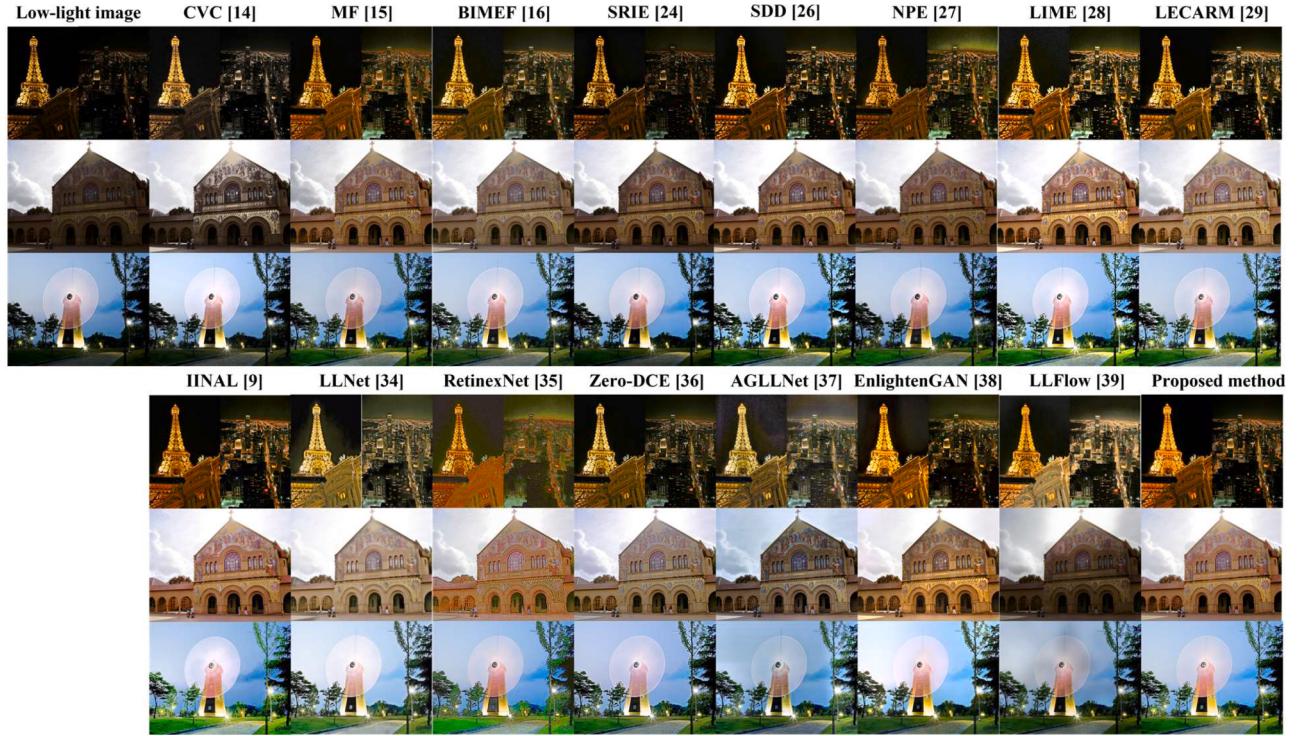


Fig. 7. Low-light image restoration results for DICM dataset [43].

of the images. NPE achieved an acceptable brightness recovery, but with slightly low image detail. However, although LIME achieved a reasonable enhancement performance, under- and over-enhancement were observed in the sample images. The results of BIMEF show acceptable performance despite slightly lower brightness recovery. IINAL produces reasonably enhanced images with a slight over-enhanced detail. LLNet

achieves good brightness restoration despite reduced detail recovery and a faint color. Furthermore, RetinexNet generates significant color shifts and unrealistic artifacts. The enhanced results obtained using Zero-DCE exhibit a slightly lower brightness recovery and weak detail information. AGLLNet generates undesirable artifacts in restored images. Although EnlightenGAN exhibited good brightness recovery, it

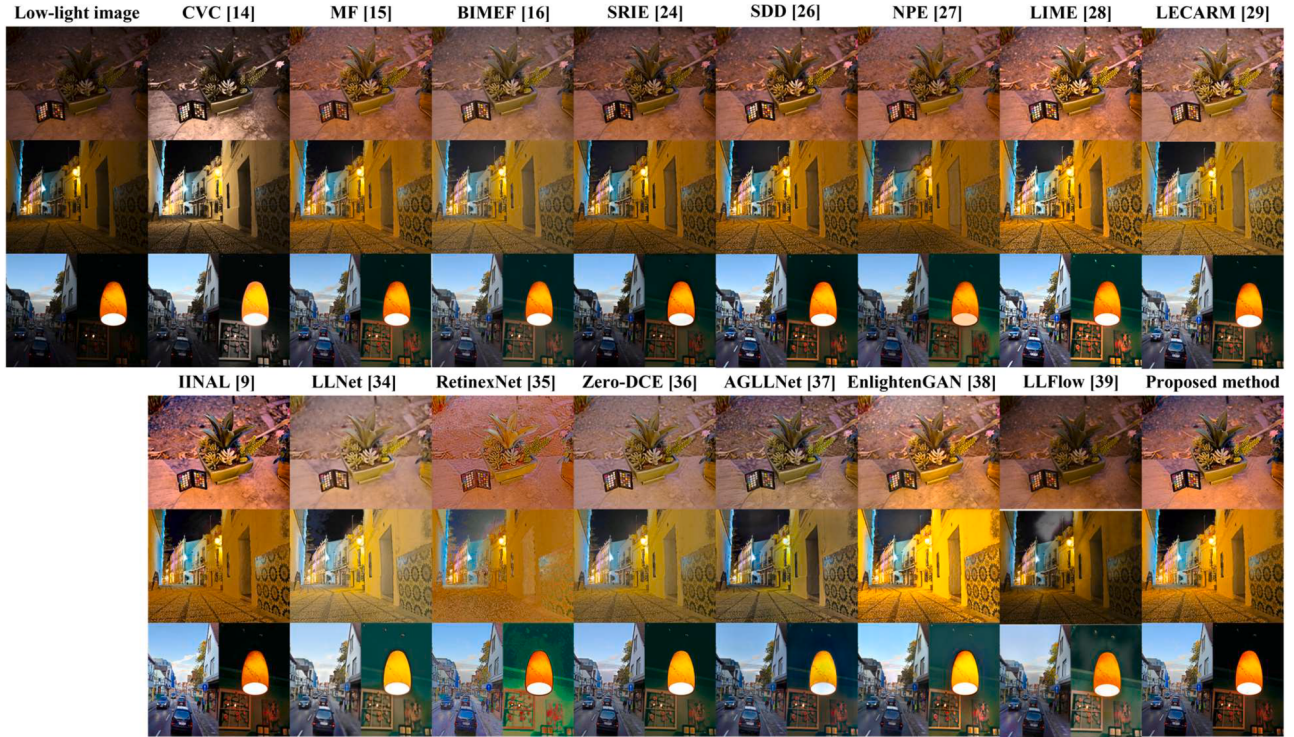


Fig. 8. Low-light image restoration results for LIME dataset [28].

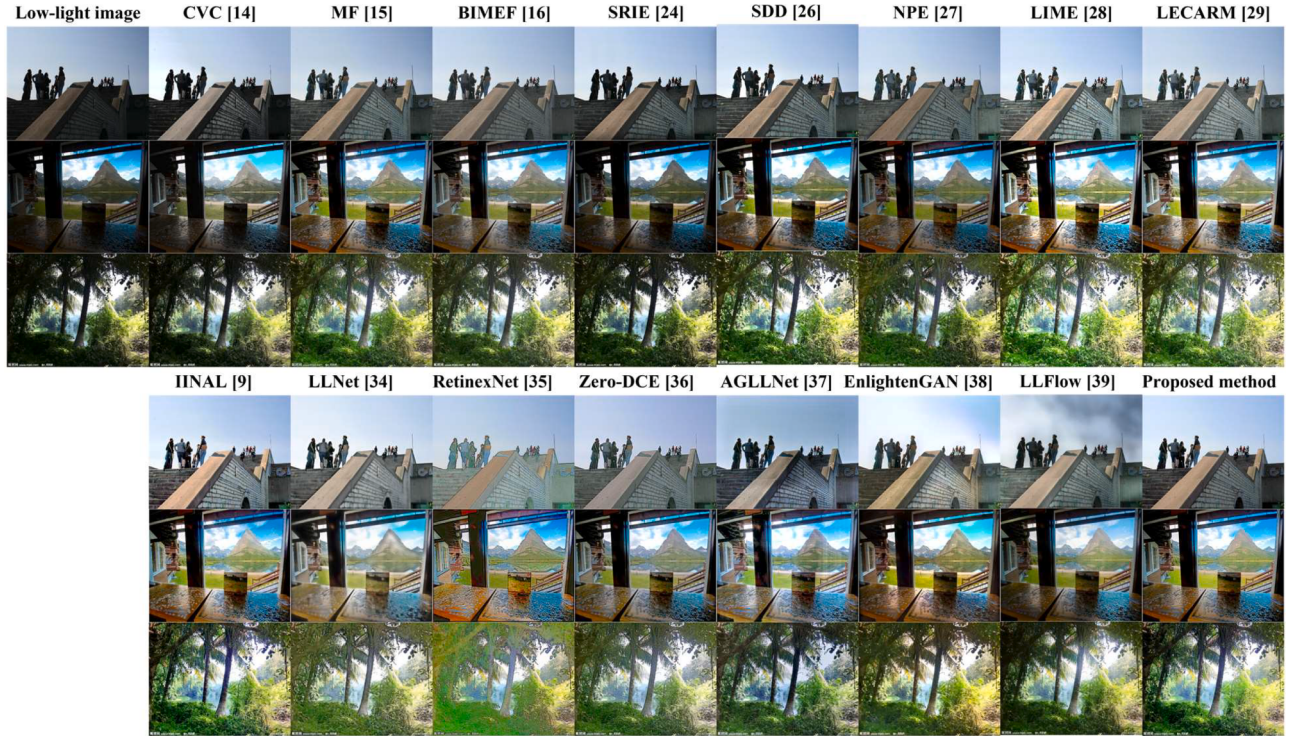


Fig. 9. Low-light image restoration results for Fusion dataset [44].

produces a color shift that cannot be ignored. LLFlow exhibits a weak brightness recovery and the effect of smudging light black. Conversely, the proposed method exhibits an acceptable recovery performance for color information while producing high brightness. It also effectively restores the details of the image within a short execution time.

4.3. Qualitative comparison

For a qualitative comparison, we used four public datasets with no-reference images: DICM (44 images) [43], LIME (10 images) [28], Fusion (16 images) [44], and VV (24 images) [45]. Enhanced low-light images can be examined regarding brightness recovery, color



Fig. 10. Low-light image restoration results for VV dataset [45].

restoration, and the recovery of image details.

Fig. 7 presents a qualitative comparison of the results of our proposed method with those of state-of-the-art LIE methods for the DICM dataset. As shown in Fig. 7, CVC fails to recover brightness. The enhanced images obtained using CVC exhibit results consistent with the quantitative scores shown in Fig. 6 and Table 2. The results obtained for MF and NPE exhibit a color shift in very low intensity regions. SRIE does not fully recover the brightness of the images. Moreover, BIMEF does not fully recover the brightness of the images and shows dimmed color. SDD does not produce the expected results despite its high computational costs. Although LIME generates good visual quality, it tends to produce over-enhanced images. LECARM and IINAL achieve good visual quality. LLNet achieves acceptable brightness, however, it has a significant color shift. Machine learning-based methods, including LLNet and RetinexNet produce unrealistic enhanced images for natural test images. Furthermore, although results obtained for Zero-DCE and AGLLNet exhibit reasonable brightness recovery, they produce faint color and unrealistic artifacts. EnlightenGAN shows good image details and reasonable brightness. LLFlow exhibits slight smudging artifacts. However, the proposed method provides acceptable brightness, image details, and color information.

The LIE results for the LIME, Fusion, and VV datasets are illustrated in Figs. 8, 9, and 10, respectively. The enhanced results of these three datasets also tended to be identical to the results of the DICM dataset shown in Fig. 7. In summary, the LIE results obtained using the proposed scheme are comparable or superior to those of the existing methods regarding brightness, detail, and color recovery. When considering computation times, the advantages of the proposed method are considerable.

For further comparison, non-reference image quantitative evaluation measures are used to verify the performance of the enhanced images. These are the naturalness image quality evaluator (NIQE) [46], the no-reference image quality metric for contrast distortion (NIQMC) [47], and the blind/referenceless image spatial quality evaluator (BRISQUE) [48]. The NIQE is a popular blind image quality assessment measure based on the construction of a quality-aware collection of statistical

features, derived from a simple and successful space-domain natural scene statistical model. The NIQMC can determine the advanced contrast and better-quality image between the two images. BRISQUE yields a measure of visual quality using a natural scene statistics-based distortion-generic blind/no-reference image quality assessment model that operates in the spatial domain. For NIQE and BRISQUE, lower values represent higher image quality, and for NIQMC, higher values indicate enhanced image quality.

Fig. 11 illustrates representative image enhancement results, enlarged versions, and evaluation metrics for two sample low-light images. LEGARM and IINAL demonstrate excellent NIQE and NIQMC scores, but the BRISQUE score is not satisfactory. However, the enhanced images are considered acceptable. The color restoration in Zero-DCE is unsatisfactory and the three scores are not outstanding. EnlightenGAN ends to generate overly enhanced images and faces challenges in accurately restoring the image details. Consequently, all the scores for EnlightenGAN are unsatisfactory. AGLLNet faces challenges in color restoration, and it tends to excessively enhance the images. LLFlow struggles to achieve successful brightness restoration and encounters difficulties in recovering image details. Although the NIQE score of the image improved by LLFlow is excellent, the other two scores are not satisfactory. In contrast, the images restored by the proposed method exhibit excellent color and brightness restoration, along with acceptable preservation of image details. Moreover, the scores obtained by the proposed method are highly competitive compared to other methods.

Table 3 shows a comparison of the average NIQE values for the four datasets. The LLFlow is shown to have the best average NIQE score, followed by EnlightenGAN and proposed method. The average NIQE values of LLNet and RetinexNet, which exhibit unrealistic enhancement results, are significantly higher than those of the other methods. Table 4 presents the average NIQMC scores for the four datasets. The maximum NIQMC scores are obtained by IINAL. Since the NIQMC assesses image quality by measuring the local details and global histogram of the given image, a high NIQMC score can be obtained for images with increased contrast or over-enhancement. Therefore, enhancement methods are

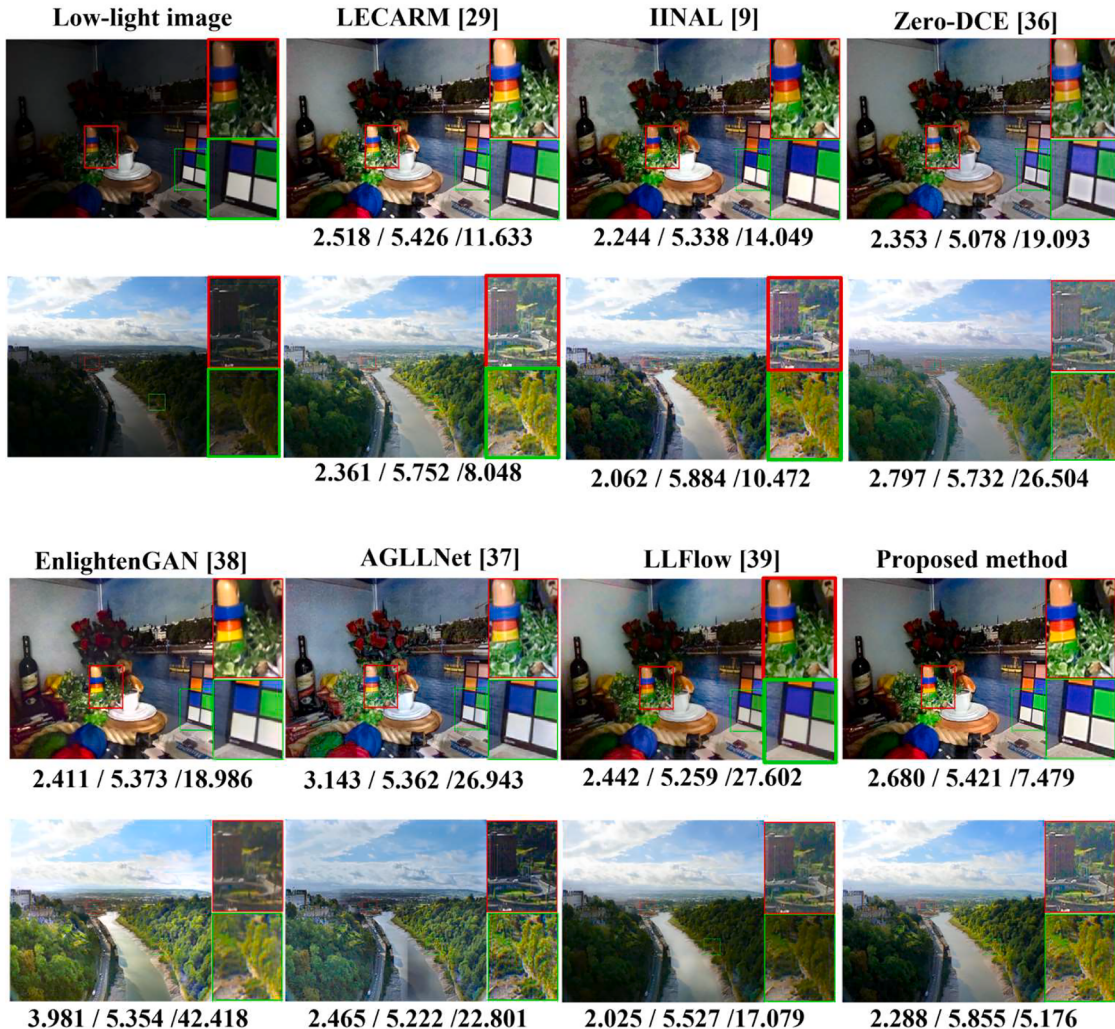


Fig. 11. Low-light image restoration results and enlarged versions. The three numbers below the reconstructed image represent NIQE, NIQMC, and BRISQUE, respectively.

Table 3

Average NIQE [46] values for four datasets.

| Method | NIQE ↓ | | | | |
|-------------------|--------------|--------------|--------------|--------------|--------------|
| | DICM | LIME | Fusion | VV | Average |
| CVC [14] | 3.470 | 4.030 | 3.567 | 2.693 | 3.440 |
| MF [15] | 3.414 | 4.067 | 3.420 | 2.579 | 3.370 |
| BIMEF [16] | 3.340 | 3.860 | 3.435 | 2.808 | 3.361 |
| SRIE [24] | 3.289 | 3.786 | 3.567 | 2.849 | 3.373 |
| SDD [26] | 3.895 | 4.383 | 4.177 | 3.412 | 3.967 |
| NPE [27] | 3.377 | 3.905 | 3.376 | 2.525 | 3.296 |
| LIME [28] | 3.430 | 4.109 | 3.601 | 2.494 | 3.409 |
| LECARM [29] | 3.334 | 3.912 | 3.440 | 2.629 | 3.329 |
| IINAL [9] | 3.320 | 3.994 | 3.322 | 2.499 | 3.284 |
| LLNet [34] | 4.584 | 4.943 | 4.679 | 4.447 | 4.663 |
| RetinexNet [35] | 4.500 | 4.591 | 4.256 | 2.693 | 4.010 |
| Zero-DCE [36] | 2.827 | 3.803 | 3.560 | 3.209 | 3.350 |
| AGLLNet [37] | 3.114 | 4.283 | 3.412 | 2.821 | 3.408 |
| EnlightenGAN [38] | <u>2.767</u> | <u>3.340</u> | <u>2.750</u> | 3.584 | <u>3.110</u> |
| LLFlow [39] | <u>2.503</u> | <u>3.646</u> | <u>2.822</u> | <u>2.135</u> | <u>2.776</u> |
| Proposed method | 3.513 | 4.086 | 3.229 | <u>2.091</u> | 3.230 |

shown to produce undesirable over-enhancements. However, this evaluation measure does not consider how well the brightness recovery of the image has been performed and whether it has an unrealistic artifact. Table 5 lists the average BRISQUE scores. The proposed algorithm achieved the highest ranking. The CVC, LECARM, and LLFlow had high

Table 4

Average NIQMC [47] values for four datasets.

| Method | NIQMC ↑ | | | | |
|-------------------|--------------|--------------|--------------|--------------|--------------|
| | DICM | LIME | Fusion | VV | Average |
| CVC [14] | 5.135 | 4.997 | <u>5.300</u> | 5.394 | 5.207 |
| MF [15] | 5.212 | 4.869 | 5.198 | <u>5.481</u> | 5.190 |
| BIMEF [16] | 5.078 | 4.721 | 5.067 | 5.285 | 5.038 |
| SRIE [24] | 4.892 | 4.503 | 4.983 | 5.295 | 4.918 |
| SDD [26] | 5.160 | 4.824 | 4.311 | 5.278 | 4.893 |
| NPE [27] | 5.089 | 4.617 | 5.072 | 5.236 | 5.004 |
| LIME [28] | <u>5.433</u> | <u>5.331</u> | 4.688 | 5.479 | 5.233 |
| LECARM [29] | 5.257 | 5.082 | 5.216 | 5.432 | 5.247 |
| IINAL [9] | 5.343 | 5.186 | <u>5.356</u> | <u>5.546</u> | <u>5.358</u> |
| LLNet [34] | 5.236 | 5.245 | 5.031 | 5.430 | 5.236 |
| RetinexNet [35] | 4.907 | 5.080 | 4.697 | 5.078 | 4.941 |
| Zero-DCE [36] | 5.113 | 5.203 | 4.834 | 5.395 | 5.136 |
| AGLLNet [37] | <u>5.353</u> | <u>5.247</u> | 4.940 | <u>5.497</u> | <u>5.259</u> |
| EnlightenGAN [38] | 5.247 | 5.089 | 5.228 | 5.448 | 5.253 |
| LLFlow [39] | 5.166 | 5.014 | 5.224 | 5.441 | 5.211 |
| Proposed method | 5.230 | 5.017 | 5.236 | 5.458 | 5.235 |

BRISQUE scores.

In Tables 3–5, the score significantly varies, depending on the quality measure for each LIE algorithm. EnlightenGAN showed positive evaluation results for NIQE and NIQMC. However, it had a significantly negative evaluation for BRISQUE. AGLLNet only achieved a good

Table 5

Average brisque [48] values for four datasets.

| Method | BRISQUE ↓ | | | | |
|-------------------|---------------|---------------|---------------|---------------|---------------|
| | DICM | LIME | Fusion | VV | Average |
| CVC [14] | 21.114 | 22.589 | 20.428 | 21.766 | <u>21.474</u> |
| MF [15] | 22.959 | 22.298 | 22.132 | 22.781 | 22.543 |
| BIMEF [16] | 22.795 | 23.135 | 20.742 | 22.542 | 22.304 |
| SRIE [24] | 22.545 | 24.181 | 22.402 | 24.435 | 23.391 |
| SDD [26] | 26.388 | 30.072 | 25.307 | 25.143 | 26.728 |
| NPE [27] | 21.993 | 22.157 | 21.805 | 22.818 | 22.193 |
| LIME [28] | 24.128 | 23.572 | 22.860 | 25.395 | 23.989 |
| LECARM [29] | 22.269 | 21.964 | 19.629 | 22.936 | 21.700 |
| IINAL [9] | 22.387 | 22.634 | 23.111 | 24.280 | 23.103 |
| LLNet [34] | 39.943 | 30.475 | 35.475 | 31.471 | 34.341 |
| RetinexNet [35] | 26.637 | 26.101 | 25.743 | <u>22.463</u> | 25.236 |
| Zero-DCE [36] | 25.096 | 23.456 | 29.022 | 30.798 | 27.093 |
| AGLLNet [37] | 21.606 | 24.108 | <u>20.292</u> | 24.108 | 22.529 |
| EnlightenGAN [38] | 22.456 | <u>20.726</u> | 21.560 | 39.924 | 26.167 |
| LLFlow [39] | 18.133 | 23.343 | 22.411 | 23.059 | 21.737 |
| Proposed method | <u>20.815</u> | 18.868 | 22.021 | <u>20.475</u> | 20.545 |

Table 6Non-reference image quantitative evaluation metrics for difference Γ_{\max} values.

| | PSNR↑ | SSIM↑ | CIEDE 2000↓ |
|-------------------|--------|-------|-------------|
| $\Gamma_{\max}=5$ | 19.087 | 0.720 | 11.853 |
| $\Gamma_{\max}=6$ | 18.808 | 0.717 | 12.034 |
| $\Gamma_{\max}=7$ | 18.475 | 0.713 | 12.307 |
| $\Gamma_{\max}=8$ | 18.140 | 0.708 | 12.618 |

NIQMC score. The proposed method, IINAL, LECARM, and LLFlow obtain reasonable scores for all the presented three image quality measures. Therefore, the proposed method generates a reasonable performance for no- and full-reference image quality measures.

4.4. Ablation study

We conduct two ablation experiments to assess the influence of different Γ_{\max} values and evaluate the effectiveness of the proposed transmission map estimation method. Table 6 presents the enhancement results obtained by varying the Γ_{\max} values using the GLADNet dataset [40]. As observed in Table 6, it is evident that when $\Gamma_{\max}=5$, the values of the three non-reference evaluation metrics are at their best. While there is a slight decrease in the objective values with increasing Γ_{\max} values, it is important to note that the results with $\Gamma_{\max}=6$ are presented in this paper, taking into account subjective image quality.

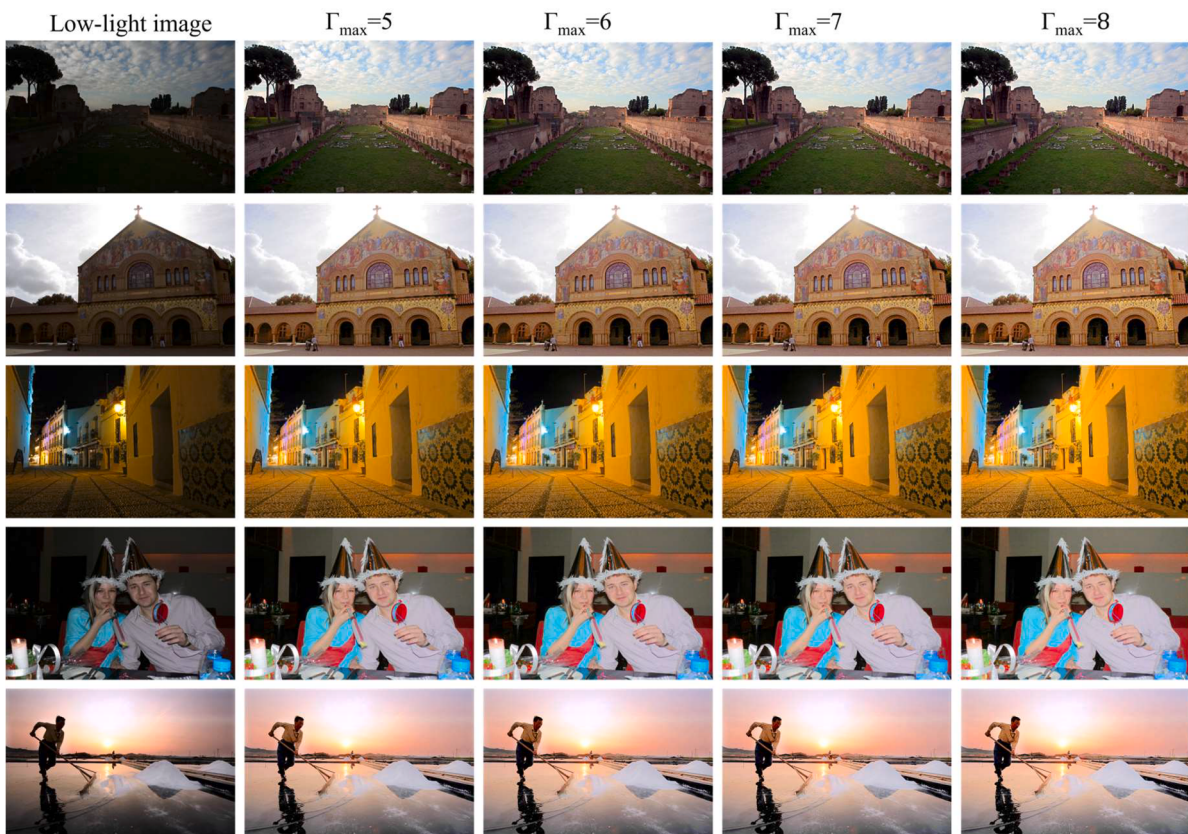
Fig. 12 shows restored images obtained by varying the Γ_{\max} values. In Fig. 12, it is evident that the brightness of the restored image increases as the gamma value increases. A Γ_{\max} value of 5 may yield favorable objective metrics, but it results in slightly dark output images. Conversely, if the Γ_{\max} value is excessively large, there is a risk of over-enhancement. Therefore, in this paper, we choose $\Gamma_{\max}=6$ that ensures significant improvement while maintaining an acceptable objective value. Moreover, as the difference in image quality due to changes in the Γ_{\max} value is not substantial, the proposed method with only one parameter can generate relatively stable results.

To assess the effectiveness of the proposed method utilizing two saturation components, we obtain enhanced images using both the proposed transmission map as described in (25) and the simplified map

Table 7

Performance comparison between the proposed method and the direct application of (6) for enhancing low-light images.

| | PSNR↑ | SSIM↑ | CIEDE 2000↓ |
|-----------------------------------|--------|-------|-------------|
| Directly applied $t(x)$ using (6) | 16.754 | 0.683 | 14.184 |
| Proposed $t(x)$ using (25) | 18.808 | 0.717 | 12.034 |

Fig. 12. Low-light image restoration results obtained by varying Γ_{\max} values.

from (6). GCP is used to calculate each of these maps for the evaluation. Table 7 presents the objective measurement values obtained using the proposed transmission map and the directly applied map for the GLADNet dataset. As depicted in Table 7, the proposed method demonstrates significantly superior values for all three metrics compared to the directly applied method. In conclusion, the proposed method, which incorporates two saturation components and utilizes GCP for transmission map estimation, proves to be effective in enhancing low-light images.

5. Conclusion

In this paper, we proposed an efficient and fast low-light image enhancement method. The main contribution of this paper was the analytical induction of a spatially-adaptive transmission map through the integration of two saturation components in a mixed color space. Additionally, the estimation of the gamma value, which plays a crucial role in determining the transmission map, was estimated using the gamma correction prior. The simulation results demonstrated that the proposed method exhibited superior performance in terms of full-reference image quality measures and delivered satisfactory results for no-reference image quality measures. Overall, the proposed low-light image enhancement scheme surpassed state-of-the-art approaches in terms of computational simplicity and enhancement efficiency. We believe that the proposed method has the potential to serve as a pre-processing technique for enhancing performance in various computer vision domains. Its effectiveness and versatility can inspire further research and development, leading to the exploration of new applications in the field. In the future, we will endeavor to design a machine learning-based low-light image enhancement network using knowledge from the proposed model-based method.

Declaration of Competing Interest

We confirm that this work is original and has not been published elsewhere nor is it currently under consideration for publication elsewhere. We have no conflicts of interest to disclose.

Data availability

Data will be made available on request.

References

- [1] H. Wang, Y. Chen, Y. Cai, L. Chen, Y. Li, M.A. Sotelo, Z. Li, SFNet-N: an improved SFNet algorithm for semantic segmentation of low-light autonomous driving road scenes, *IEEE Trans. Intell. Transp. Syst.* 23 (11) (2022) 21405–21417, <https://doi.org/10.1109/TITS.2022.3177615>.
- [2] V. Crescittelli, A. Kosuge, T. Oshima, POISON: human pose estimation in insufficient lighting conditions using sensor fusion, *IEEE Trans. Instrum. Meas.* 70 (2021), 2504408, <https://doi.org/10.1109/TIM.2020.3043872>.
- [3] K. Guo, M. Hu, S. Ren, F. Li, Zhang J, H. Guo, X. Kui, Deep illumination-enhanced face super-resolution network for low-light images, *ACM Trans. Multimedia Comput. Commun. Appl.* 18 (3) (2022), 87, <https://doi.org/10.1145/3495258>.
- [4] W. Wang, X. Wu, X. Yuan, Z. Gao, An experiment-based review of low-light image enhancement methods, *IEEE Access* 8 (2020) 87884–87917, <https://doi.org/10.1109/ACCESS.2020.2992749>.
- [5] C. Li, C. Guo, L. Han, J. Jiang, M.M. Cheng, J. Gu, C.C. Loy, Low-light image and video enhancement using deep learning: a survey, *IEEE Trans. Pattern Anal. Mach. Intell.* 44 (12) (2022) 9396–9416, <https://doi.org/10.1109/TPAMI.2021.3126387>.
- [6] M. Veluchamy, A.K. Bhandari, B. Subramani, Optimized Bezier curve based intensity mapping scheme for low light Image enhancement, *IEEE Trans. Emerg. Top. Comput. Intell.* 6 (3) (2022) 602–612, <https://doi.org/10.1109/TETCI.2021.3053253>.
- [7] N. Singh, A.K. Bhandari, Multiscale reflection component based weakly illuminated nighttime image enhancement, *Circuits Syst. Signal Process.* 41 (2022) 6862–6884, <https://doi.org/10.1007/s00034-022-02080-w>.
- [8] X. Ren, W. Yang, W.-H. Cheng, J. Liu, LR3M: robust low-light enhancement via low-rank regularized Retinex model, *IEEE Trans. Image Process.* 29 (2020) 5862–5876, <https://doi.org/10.1109/TIP.2020.2984098>.
- [9] J.J. Jeon, I.K. Eom, Low-light image enhancement using inverted image normalized by atmospheric light, *Signal Process.* 196 (2022), 108523, <https://doi.org/10.1016/j.sigpro.2022.108523>.
- [10] M. Ju, C. Ding, Y.J. Guo, D. Zhang, IDGCP: image dehazing based on gamma correction prior, *IEEE Trans. Image Process.* 29 (2020) 3104–3118, <https://doi.org/10.1109/TIP.2019.2957852>.
- [11] S.C. Liu, S. Liu, H. Wu, M.A. Rahman, S.C.-F. Lin, C.Y. Wong, N. Kwok, H. Shi, Enhancement of low illumination images based on an optimal hyperbolic tangent profile, *Comput. Electr. Eng.* 70 (2018) 538–550, <https://doi.org/10.1016/j.compeleceng.2017.08.026>.
- [12] K. Srinivas, A.K. Bhandari, Low light image enhancement with adaptive sigmoid transfer function, *IET Image Process.* 14 (4) (2020) 668–678, <https://doi.org/10.1049/iet-ijpr.2019.0781>.
- [13] K. Singh, R. Kapoor, Image enhancement using exposure based subimage histogram equalization, *Pattern Recogn. Lett.* 36 (2014) 10–14, <https://doi.org/10.1016/j.patrec.2013.08.024>.
- [14] T. Celik, T. Tjahjadi, Contextual and variational contrast enhancement, *IEEE Trans. Image Process.* 20 (12) (2011) 3431, <https://doi.org/10.1109/TIP.2011.2157513>.
- [15] X. Fu, D. Zeng, Y. Huang, Y. Liao, X. Ding, J. Paisley, A fusion-based enhancing method for weakly illuminated images, *Signal Process.* 129 (2016) 82–96, <https://doi.org/10.1016/j.sigpro.2016.05.031>.
- [16] Z. Ying, G. Li, W. Gao, A bio-inspired multi-exposure fusion framework for low-light image enhancement, *arXiv preprint* (2017), doi:10.48550.arXiv.1711.00591.
- [17] H.D. Cheng, M. Xue, X.J. Shi, Contrast enhancement based on a novel homogeneity measurement, *Pattern Recogn.* 36 (11) (2003) 2687–2697, [https://doi.org/10.1016/S0031-3203\(03\)00054-2](https://doi.org/10.1016/S0031-3203(03)00054-2).
- [18] J. Mukherjee, S.K. Mitra, Enhancement of color images by scaling the DCT coefficients, *IEEE Trans. Image Process.* 17 (10) (2008) 1783–1794, <https://doi.org/10.1109/TIP.2008.2002826>.
- [19] S.E. Kim, J.J. Jeon, I.K. Eom, Image contrast enhancement using entropy scaling in wavelet domain, *Signal Process.* 127 (2016) 1–11, <https://doi.org/10.1016/j.sigpro.2016.02.016>.
- [20] E.H. Land, The Retinex theory of color vision, *Sci. Amer.* 237 (6) (1977) 108–128, <https://doi.org/10.1038/scientificamerican1277-108>.
- [21] D.J. Jobson, Z. Rahman, G.A. Woodell, Properties and performance of a center/surround Retinex, *IEEE Trans. Image Process.* 6 (3) (1997) 451–462, <https://doi.org/10.1109/83.557356>.
- [22] D.J. Jobson, Z. Rahman, A multiscale Retinex for bridging the gap between color images and the human observation of scenes, *IEEE Trans. Image Process.* 6 (7) (1997) 965–976, <https://doi.org/10.1109/83.597272>.
- [23] R. Kimmel, M. Elad, D. Shaked, R. Keshet, I. Sobel, A variational framework for Retinex, *Int. J. Comput. Vis.* 52 (1) (2003) 7–23, <https://doi.org/10.1023/A:1022314423998>.
- [24] X. Fu, Y. Liao, D. Zeng, Y. Huang, X.-P. Zhang, X. Ding, A probabilistic method for image enhancement with simultaneous illumination and reflectance estimation, *IEEE Trans. Image Process.* 24 (12) (2015) 4965–4977, <https://doi.org/10.1109/TIP.2015.2474701>.
- [25] M. Li, J. Liu, W. Yang, X. Sun, Z. Guo, Structure-revealing low-light image enhancement via robust Retinex model, *IEEE Trans. Image Process.* 27 (6) (2018) 2828–2841, <https://doi.org/10.1109/TIP.2018.2810539>.
- [26] S. Hao, X. Han, Y. Guo, X. Xu, M. Wang, Low-light image enhancement with semi-coupled decomposition, *IEEE Trans. Multimedia* 22 (12) (2020) 3025–3038, <https://doi.org/10.1109/TMM.2020.2969790>.
- [27] S. Wang, J. Zheng, H.-M. Hu, B. Li, Naturalness preserved enhancement algorithm for non-uniform illumination images, *IEEE Trans. Image Process.* 22 (9) (2013) 3538–3578, <https://doi.org/10.1109/TIP.2013.2261309>.
- [28] X. Guo, Y. Li, H. Ling, LIME: low-light image enhancement via illumination map estimation, *IEEE Trans. Image Process.* 26 (2) (2017) 982–993, <https://doi.org/10.1109/TIP.2016.2639450>.
- [29] Y. Ren, Z. Ying, T.H. Li, G. Li, LECARM: low-light image enhancement using the camera response model, *IEEE Trans. Circuits Syst. Video Technol.* 29 (4) (2019) 968–981, <https://doi.org/10.1109/TCST.2018.2828141>.
- [30] S.G. Narasimhan, S.K. Nayar, Contrast restoration of weather degraded images, *IEEE Trans. Pattern Anal. Mach. Intell.* 25 (6) (2003) 713–724, <https://doi.org/10.1109/TPAMI.2003.1201821>.
- [31] Z. Shi, M. Zhu, B. Guo, M. Zhao, A photographic negative imaging inspired method for low illumination night-time image enhancement, *Multimed. Tools Appl.* 76 (2017) 15027–15048, <https://doi.org/10.1007/s11042-017-4453-z>.
- [32] K.M. He, J. Sun, X.O. Tang, Single image haze removal using dark channel prior, *IEEE Trans. Pattern Anal. Mach. Intell.* 33 (12) (2011) 2341–2353, <https://doi.org/10.1109/TPAMI.2010.168>.
- [33] Z. Gu, Chen C, D. Zhang, A low-light image enhancement method based on image degradation model and pure pixel ratio prior, *Math. Probl. Eng.* (2018), 8178109, <https://doi.org/10.1155/2018/8178109>.
- [34] K.G. Lore, A. Akintayo, S. Sarkar, LLNet: a deep autoencoder approach to natural low-light image enhancement, *Pattern Recognit.* 61 (2017) 650–662, <https://doi.org/10.1016/j.patcog.2016.06.008>.
- [35] C. Wei, W. Wang, W. Yang, J. Liu, Deep Retinex decomposition for low-light enhancement, *arXiv preprint* (2018), doi: 10.48550.arXiv.1808.04560.
- [36] C. Guo, C. Li, J. Cuo, C.C. Loy, J. Hou, S. Kwong, R. Cong, Zero-reference deep curve estimation for low-light image enhancement, in: *IEEE Conf. Comput. Vis. Pattern Recognit.*, 2020, pp. 1780–1789, <https://doi.org/10.1109/CVPR42600.2020.00185>.

- [37] F. Lv, Y. Li, F. Lu, Attention guided low-light image enhancement with a large scale low-light simulation dataset, *Int. J. Comput. Vis.* 129 (2021) 2175–2193, <https://doi.org/10.1007/s11263-021-01466-8>.
- [38] Y. Jiang, X. Gong, D. Liu, Y. Cheng, X. Shen, J. Yang, P. Zhou, Z. Wang, EnlightenGAN: deep light enhancement without paired supervision, *IEEE Trans. Image Process.* 30 (2021) 2340–2349, <https://doi.org/10.1109/TIP.2021.3051462>.
- [39] Y. Wang, R. Wan, H. Li, L.P. Chau, A. Kot, Low-light image enhancement with normalizing flow, in: AAAI Conference on Artificial Intelligence 36, 2022, pp. 2604–2612, <https://doi.org/10.1609/aaai.v36i3.20162>.
- [40] W. Wang, C. Wei, W. Yang, J. Liu, GLADNet: low-light enhancement network with global awareness, in: IEEE International Conference on Automatic Face & Gesture Recognition, 2018, pp. 751–755, <https://doi.org/10.1109/FG.2018.000118>.
- [41] Z. Wang, A.C. Bovik, H.R. Sheikh, E.P. Simoncelli, Image quality assessment: from error visibility to structural similarity, *IEEE Trans. Image Process.* 13 (4) (2004) 600–612, <https://doi.org/10.1109/TIP.2003.819861>, 2004.
- [42] G. Sharma, W. Wu, and E.N. Dalal, The ciede2000 color difference formula: implementation notes, supplementary test data, and mathematical observations, *Color Res. Appl.* 30 (1) 21–30. doi:[10.1002/col.20070](https://doi.org/10.1002/col.20070).
- [43] Q. Wang, X. Fu, X.-P. Zhang, X. Ding, A fusion-based method for single backlit image enhancement, in: IEEE Int. Conf. Image Process., 2016, pp. 4077–4081, <https://doi.org/10.1109/ICIP.2016.7533126>.
- [44] C. Lee, C. Lee, C.S. Kim, Contrast enhancement based on layered difference representation, in: IEEE Int. Conf. Image Process., 2012, pp. 965–968, <https://doi.org/10.1109/ICIP.2012.6467022>.
- [45] V. Vonikakis, Dataset. <https://sites.google.com/site/vonikakis/datasets>. (Accessed 3 November 2022).
- [46] A. Mittal, R. Soundararajan, A.C. Bovik, Making a ‘completely blind’ image quality analyzer, *IEEE Signal Process. Lett.* 20 (3) (2013) 209–212, <https://doi.org/10.1109/LSP.2012.2227726>.
- [47] K. Gu, W. Lin, G. Zhai, X. Yang, W. Zhang, C.W. Chen, No-reference quality metric of contrast-distorted images based on information maximization, *IEEE Trans. Cybern.* 47 (12) (2017) 4559–4565, <https://doi.org/10.1109/TCYB.2016.2575544>.
- [48] A. Mittal, A.K. Moorthy, A.C. Bovik, No-reference image quality assessment in the spatial domain, *IEEE Trans. Image Process.* 21 (12) (2012) 4695–4708, <https://doi.org/10.1109/TIP.2012.2214050>, orted images based on information maximization, *IEEE Trans. Cybern.* 47 (12) (2017) 4559–4565. 10.1109/TCYB.2016.2575544.

Jong Ju Jeon received the B.S. and Ph.D degrees from the Department of Electronics Engineering at Pusan National University, South Korea, in 2014, 2023, respectively. He is currently employed at the National Forensic Service in South Korea. His research interests primarily revolve around computer vision and image processing. His research interests include computer vision and image processing.

Jun Young Park received the B.S. degree from the Department of Electronics Engineering at Pusan National University, South Korea, in 2017. Currently, he is pursuing a Ph.D. in Electronics Engineering at Pusan National University. His research interests encompass computer vision, machine learning, and image processing.

Il Kyu Eom received his B.S., M.S., and Ph.D. degrees from the Department of Electronics Engineering at Pusan National University, South Korea, in 1990, 1992, and 1998, respectively. From 1997 to 2005, he served as a faculty member at Miryang National University, South Korea. Since 2006, he has been a full professor at the Department of Electronics Engineering at Pusan National University. His research interests encompass image processing, computer vision, digital image forensics, and machine learning.